Available online at www.sciencedirect.com
SCIENCE DIRECT®
Acta Materialia 52 (2004) 1745–1760
Acta MATERIALIA
www.actamat-journals.com

Level set simulations of dislocation-particle bypass mechanisms

Yang Xiang [a,*,1], D.J. Srolovitz [b], L.-T. Cheng [c], Weinan E [d]

[a] Department of Mathematics, Hong Kong University of Science and Technology, Clear Water Bay, Kowloon, Hong Kong
[b] Department of Mechanical and Aerospace Engineering, Princeton Materials Institute, Princeton University, Princeton, NJ 08544, USA
[c] Department of Mathematics, University of California, San Diego, La Jolla, CA 92093, USA
[d] Department of Mathematics and PACM, Princeton University, Princeton, NJ 08544, USA

Received 17 August 2003; received in revised form 9 December 2003; accepted 12 December 2003

Abstract

Particle dispersions strengthen metals by acting as barriers to the motion of dislocations. A full analysis of the mechanisms by which dislocations bypass particles has been hindered because of complexities associated with elastic interactions between dislocation segments, their interactions with particle stress field, the flexibility of the dislocation line in three dimensions and the three-dimensional topological changes that occur. We present the results of full three-dimensional dislocation dynamics simulations, based on the level set method, that naturally accounts for all of these issues. We examine bypass mechanisms for penetrable, misfitting particles and impenetrable particles, with and without a misfit. The simulations show a wide range of bypass mechanisms, including particle cutting, dislocation loop formation and combinations of these. Loops are observed to form in front of and behind particles, on the sides of particles, in between particles, around particles and as combinations of these. Some of the bypass mechanisms are classical and others have never been reported previously. We also observe a novel dislocation multiplication mechanism associated with misfitting particles. The observations are compared with those in the literature and from previous theories and simulations.

Keywords: Dislocation dynamics; Simulation; Plastic deformation; Dislocations

1. Introduction

The addition of a particle dispersion to metals is a common strategy used to strengthen alloys. The question of how these dispersoids strengthen metals has been examined since the early days of dislocation theory and transmission electron microscopy (TEM). The microscopic origin of the particle strengthening has its roots in dislocation theory and is associated with the particles serving as obstacles to dislocation motion. Dislocations can bypass particles by Orowan loop [1], particle cutting, or cross-slip [2] mechanisms. The operative bypass mechanism depends on the nature of the dislocation-particle interactions (such as hard core repulsion, particle misfit stress fields, modulus difference-induced stresses, defect formation upon particle cutting, etc.), the relative locations of the particles and slip planes, and whether the dislocation is an edge or screw. In realistic situations, the situation is further complicated by the fact that dislocations can be of mixed type (neither pure edge or screw), the availability of multiple slip planes, and the fact that the different bypass mechanisms can operate in concert. Many analytic analyses of the bypass process have been discussed [1–7] and numerical simulations performed [8–16]. Most of these analyses focused on the motion of dislocations constrained to a single slip plane, where dislocations bypass particles by either Orowan looping or particle cutting. In addition, particle bypassing by a cross-slip mechanism was used successfully to explain the qualitative features of the formation of prismatic loops observed in experiments [2,7,17–19]. No numerical simulations of this cross-slip mechanism have been performed, nor has cross-slip been considered in simulations designed to obtain the critical stress for dislocations to bypass particles. MacEwen et al. [20] did

* Corresponding author. Tel.: +852-23587430; fax: +852-23581643.
E-mail address: maxiang@ust.hk (Y. Xiang).
[1] Formerly at Princeton Materials Institute, Princeton University, Princeton, NJ 08544, USA.

1359-6454/$30.00 © 2004 Acta Materialia Inc. Published by Elsevier Ltd. All rights reserved.
doi:10.1016/j.actamat.2003.12.016

perform a numerical analysis of this situation but because their calculations were limited to two spatial dimensions, several assumptions had to be used to determine when cross-slip loops were actually formed.

In this paper, we simulate dislocations bypassing impenetrable particles and misfitting particles (both impenetrable and penetrable) for different positions of the slip plane relative to the center of the particle and for different Burgers vectors. The simulation method we used is the level set method for dislocation dynamics proposed by the present authors in [21], which naturally accounts for glide along the slip plane and cross-slip of screw segments. The focus of this study is to identify the dominant bypass mechanisms and describe how they operate. Several of the mechanisms seen in these simulations have been observed experimentally and some are entirely new (to our knowledge).

2. Level set simulation method

We simulate the motion of an initially straight dislocation, moving under an applied stress, towards a periodic array of particles. The simulations are performed for the impenetrable, non-misfitting particles as well as misfitting particles which are either penetrable or impenetrable. We consider both initially pure edge and pure screw dislocations that glide on slip planes that intersect the particles at different heights (for the case of the screw dislocation, we refer to the plane upon which the dislocation would glide in the given applied stress in the absence of the particle array). The simulations are performed within the level set, dislocation dynamics framework that the present authors described earlier [21]. The method is briefly summarized here. More details of the dislocation theory and level set method can be found in the following references [22–28].

In the level set method for dislocation dynamics [21], a dislocation $\gamma(t)$ is represented by the intersection of the zero level sets of two level set functions $\phi(x,y,z,t)$ and $\psi(x,y,z,t)$ defined in the three-dimensional space, i.e., where

$$\phi(x,y,z,t) = \psi(x,y,z,t) = 0, \tag{1}$$

see Fig. 1. The evolution of the dislocation is described by the evolution of the level set functions

$$\begin{aligned} \phi_t + \mathbf{v}\cdot\nabla\phi &= 0, \\ \psi_t + \mathbf{v}\cdot\nabla\psi &= 0, \end{aligned} \tag{2}$$

where $\mathbf{v}$ is the velocity field obtained by smoothly extending the velocity of the dislocation to the full three-dimensional space.

The local dislocation velocity is given by

$$\mathbf{v} = \mathbf{M}\cdot\mathbf{f}, \tag{3}$$

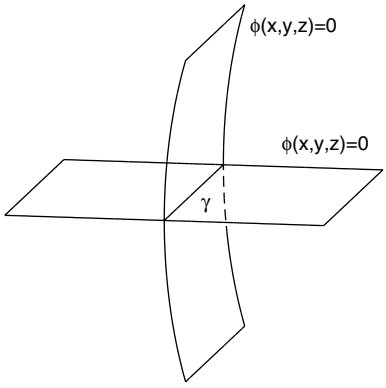

Fig. 1. A dislocation $\gamma(t)$ in the three-dimensional space is the intersection of the zero level sets of the two level set functions $\phi(x,y,z,t)$ and $\psi(x,y,z,t)$.

where $\mathbf{M}$ is the mobility tensor, $\mathbf{f}$ is the Peach–Koehler force on the dislocation. The Peach–Koehler force is

$$\mathbf{f} = \sigma^{\text{tot}}\cdot\mathbf{b}\times\xi, \tag{4}$$

where ξ is the unit tangent vector of the dislocation and σ^{tot} is the total stress which includes contributions from the self-stress σ and the applied stress σ^{appl}:

$$\sigma^{\text{tot}} = \sigma + \sigma^{\text{appl}}. \tag{5}$$

The self-stress is obtained by solving the following linear elasticity system (for simplicity, we assume the material is elastically isotropic):

$$w_{ij} = \frac{\partial u_j}{\partial x_i}, \quad i,j = 1,2,3, \tag{6}$$

$$\epsilon_{ij} = \frac{1}{2}(w_{ij} + w_{ji}), \quad i,j = 1,2,3, \tag{7}$$

$$\sigma_{ij} = 2G\epsilon_{ij} + G\frac{2v}{1-2v}(\epsilon_{11}+\epsilon_{22}+\epsilon_{33})\delta_{ij}, \quad i,j = 1,2,3, \tag{8}$$

$$\nabla\cdot\sigma = \mathbf{0}, \tag{9}$$

$$\nabla\times\mathbf{w} = \xi\delta(\gamma)\otimes\mathbf{b}, \tag{10}$$

where $\mathbf{u}$ is the elastic displacement vector, $\mathbf{w}$ is the distortion tensor, $\{\epsilon_{ij}\}$ is the strain tensor, G is the shear modulus, v is the Poisson ratio, δ_{ij} is equal to 1 if $i=j$ and 0 otherwise, $\mathbf{b}$ is the Burgers vector, the operator $\otimes$ is the tensor product operator, ξ is the unit vector tangent to the dislocation line, $\delta(\gamma)$ is the two-dimensional delta function in the plane perpendicular to the dislocation and is zero everywhere except on the dislocation.

The unit tangent vector ξ of the dislocation can be calculated from the level set functions ϕ and ψ:

$$\xi = \frac{\nabla\phi\times\nabla\psi}{|\nabla\phi\times\nabla\psi|}. \tag{11}$$

The delta function in Eq. (10) is given by

$$\delta(\gamma) = \delta(\phi)\delta(\psi), \tag{12}$$

where the delta functions on the right-hand side are one-dimensional, smeared delta functions

$$\delta(x) = \begin{cases} \dfrac{1}{2\epsilon_c}\left(1 + \cos\dfrac{\pi x}{\epsilon_c}\right), & -\epsilon_c \leqslant x \leqslant \epsilon_c, \\ 0, & \text{otherwise}, \end{cases} \tag{13}$$

and ϵ_c scales the distance over which the delta function is smeared. The region where the delta function is not zero represents the core region of the dislocation.

We now define the dislocation mobility tensor **M**. A dislocation can move conservatively (i.e., without diffusion) only in the plane containing both its tangent and Burgers vectors (i.e., the slip plane). A screw segment on a dislocation line can move in any plane containing the dislocation, since the tangent and Burgers vectors are parallel. In other words, we do not limit the dislocations to slip on any particular crystallographic plane. The only crystallographic restriction is associated with our choice of Burgers vector. This type of mobility is appropriate for most body-centered cubic materials, such as Ta, Mo, or Fe above approximately 350 K, where screw dislocations readily move on any plane (i.e., pencil glide) [29]. In the formulation, the slip plane normal vector is

$$\mathbf{n} = \frac{\xi \times \mathbf{b}}{|\xi \times \mathbf{b}|}. \tag{14}$$

The mobility tensor can be written as

$$\mathbf{M} = \begin{cases} m_{\mathrm{g}}(\mathbf{I} - \mathbf{n} \otimes \mathbf{n}) & \text{non-screw } (\xi \text{ not parallel to } \mathbf{b}), \\ m_{\mathrm{g}}\mathbf{I} & \text{screw } (\xi \text{ parallel to } \mathbf{b}), \end{cases} \tag{15}$$

where m_{g} is the dislocation glide mobility, **I** is the identity matrix, $\mathbf{I} - \mathbf{n} \otimes \mathbf{n}$ is the orthogonal projection matrix that projects vectors onto the slip plane with normal vector **n**. We consider a dislocation to be a pure screw if $|\xi \times \mathbf{b}| < 0.1$. It is a simple matter to allow climb by adding additional terms to the mobility tensor, as described in [21].

The elasticity equations associated with the dislocations are solved using the standard FFT approach. (We keep only the periodic part of the stress tensor [21], following the boundary condition suggestion of Bulatov et al. [30]). The level set evolution equations are solved using the third-order WENO method [31] for the spatial discretization and fourth-order TVD Runge–Kutta [32] for the temporal evolution.

We consider three types of particles: hard (impenetrable) spheres, misfitting (penetrable) spheres and impenetrable misfitting spheres. Penetrable (impenetrable) particles refer to the case in which the dislocation is (not) able to cross the interface from the metal into the particle. Examples of impenetrable particles include most cases of incoherent carbide or oxide particles in metals. An example of penetrable particles are the coherent Mg_2Si particles in Al. We only consider cases in which the particles have the same elastic constants as the matrix. Further, we assume that the misfit is purely dilatational, such as for γ' particles in Ni–Al solid solutions. We note, that the present simulations do not explicitly consider the dislocation structure of the particle-matrix interface, however, this could be included by explicitly depicting those structural dislocations and including dislocation–dislocation interactions as described in [21].

2.1. Case 1: Hard spherical particles

We model a hard (impenetrable) spherical particle by creating a strong repulsive force acting on any dislocation within the particle and zero force on any dislocation outside the particle. To keep this force continuous, we introduce a smooth connecting region with width dx (the grid constant) at the particle/matrix interface. More precisely, the repulsive force generated by a hard spherical particle on the dislocation is

$$\begin{cases} f_0 & \text{if } r \leqslant R, \\ f_0(R + \mathrm{d}x - r)^2/\mathrm{d}x^2 & \text{if } R < r \leqslant R + \mathrm{d}x, \\ 0 & \text{if } r > R + \mathrm{d}x, \end{cases} \tag{16}$$

where R is the radius of the spherical particle, r is the distance from a point on the dislocation line to the center of the particle. Ideally, f_0 should be $+\infty$. In our simulations, we simply choose f_0 to be large enough so that the dislocation cannot penetrate the particle.

2.2. Case 2: Misfitting spherical particles

A particle which is misfitting with respect to the matrix, generates stress fields both within the particle and in the matrix. The dislocation interacts with the particle through these stress fields. The stress fields generated by a (dilatational) misfitting spherical particle (isotropic elasticity) were given by Eshelby [33] and others. The stress field at a point outside a particle of radius R sitting at the origin of the coordinate system $(0, 0, 0)$ is

$$\sigma^{\mathrm{pt}} = \frac{2G\epsilon R^3}{r^5}\begin{pmatrix} r^2 - 3x^2 & -3xy & -3xz \\ -3xy & r^2 - 3y^2 & -3yz \\ -3xz & -3yz & r^2 - 3z^2 \end{pmatrix}, \tag{17}$$

where r is the distance from the point to the particle center, and the stress tensor inside the particle ($r < R$) is

$$\sigma^{\mathrm{pt}} = -4G\epsilon\begin{pmatrix} 1 & 0 & 0 \\ 0 & 1 & 0 \\ 0 & 0 & 1 \end{pmatrix}, \tag{18}$$

the parameter $\epsilon = \epsilon_0(1 + \nu)/3(1 - \nu)$ and ν is Poisson ration, ϵ_0 is the dilatational misfit strain. Because we enforce periodic boundary conditions, the stress

field associated with the particle at any point in the simulation cell is the result of the superposition of the stress fields of the particle within the cell and from all of the periodic images of that particle. Since the stress field decays relatively quickly away from the particle, we can replace this summation with a sum over the $9 \times 9 \times 9$ periodic cell images centered on the cell of interest without introducing significant errors.

2.3. Case 3: Impenetrable, misfitting spherical particles

This case is simply a linear combination of Cases 1 and 2. In other words, we employ the nearly hard particle repulsion of Case 1 with the misfit stress field outside the particle, as per Case 2.

The simulations are performed within simulation cells that are $l \times l \times l$, where $l = 2 = 500b$. We assume period boundary conditions and discretize the simulation cell into $64 \times 64 \times 64$ grid points. (In some cases, we use simulation cells of $2l \times l \times l$ discretized into $128 \times 64 \times 64$ grid points.) The core radius $\epsilon_c = 3\,\mathrm{d}x = 0.09375$, where $\mathrm{d}x = l/64 = 0.03125$ is the grid spacing. The core radius is 25 times larger than the actual Burgers vector. This is only a limitation if we want to resolve the problem on finer length scales. This value is chosen as a compromise between resolution and computational demands. The stresses reported herein are all scaled by $Gb/2l$, the mobility is scaled by the glide mobility m_g, and the time is scaled by $4l/Gb^2m_g$. We set the particle radius as $R = 0.4(100b)$, the Poisson ratio $v = 1/3$, the misfit parameter $\epsilon = 0.02$, and the repulsive force parameter for the impenetrable spherical particles $f_0 = 85Gb^2/l$, which is large enough to prevent the dislocation from cutting through the particles. We arbitrarily set the applied shear stress $\tau = 4Gb/2l = G/250$, which is large enough so that the dislocation can bypass the particles in all cases. For the case of body-centered cubic lattice constant $b = 0.286$ nm and $G = 161$ GPa, such that the simulation cell size is 143 nm, the particle radius is 29 nm, and the applied shear stress is 640 MPa. The absolute values of the mobility and the units of time are arbitrary, since they do not effect the reported dynamics (although the ratio of the glide to climb mobilities do).

3. Hard spherical particles

In this section, we present the simulation results for a dislocation being driven past an array of impenetrable, spherical particles with the same elastic constants as the matrix. The short-range repulsive interaction between the dislocation and the particles is given by Eq. (16). The force on a non-screw segment due to this repulsive interaction is its component on the slip plane of the segment. The force on a screw segment near a particle that tends to make it cross-slip is the total force resolved into the direction perpendicular to the dislocation line and the radius vector from the particle center to the dislocation segment. The radial component of the force from the local stress field on the screw segment near the particle is balanced by the strong short-range repulsive force.

In the simulations, the particle center is $(x_0, y_0, z_0) = (0.4, 0, 0)$ and its radius is $R = 0.4$. Initially, the dislocation (edge or screw) is straight and located at $x = 0.9$ and $z = h$ with the tangent vector pointing to the $+y$ direction. The dislocation moves towards the particle under an applied stress. For an edge dislocation, h measures the distance in the z direction between the slip plane and the plane containing the particle center. For a screw dislocation, h measures the distance in the z direction between the plane on which the dislocation would slip in the absence of the particle and the plane containing the particle center. We vary the relative positions of the particle and the slip plane of the dislocation by varying h. The case $h > 0$ or $h < 0$ implies that the slip plane is above or below the particle center, respectively. Since for hard spherical particles the $h > 0$ or $h < 0$ cases are equivalent (i.e., the problem is symmetric about $h = 0$), we only show $h \geqslant 0$ results.

3.1. Edge dislocations

In this section, we consider the case of an initially pure edge dislocation, with Burgers vector $\mathbf{b}$ in the $+x$ direction and an applied shear stress $\sigma_{xz} = 4.0$.

Fig. 2 shows a simulation of the $h = 0$ case, where the particle center is on the slip plane of the initial edge dislocation. The edge dislocation approaches the particle and then bends around it. The two dislocation segments on the sides of the particle are elastically attracted to each other (recall that they have the same Burgers vector but opposite line directions). Once these segments pass the particle, they annihilate one another, leaving behind a dislocation loop as the dislocation moves on. This is exactly the classical Orowan [1] mechanism for bypassing particles. Since the slip plane passes through the particle center, the symmetry insures that the cross-slip force on the screw segments is exactly zero.

Fig. 3 shows a simulation for the case in which the slip plane of the edge dislocation is slightly above the particle center ($h = 0.1R$). The bypass mechanism is similar to that in Fig. 2 for the case of $h = 0$: i.e., the dislocation bypasses the particle by the Orowan mechanism, leaving behind a dislocation loop as the dislocation continues moving forward. However, the loop left behind does not lie entirely in the initial slip plane. The two screw segments of the loop, on the sides of the particle, cross-slip out of the initial slip plane. Because the slip plane lies above the particle center, there are

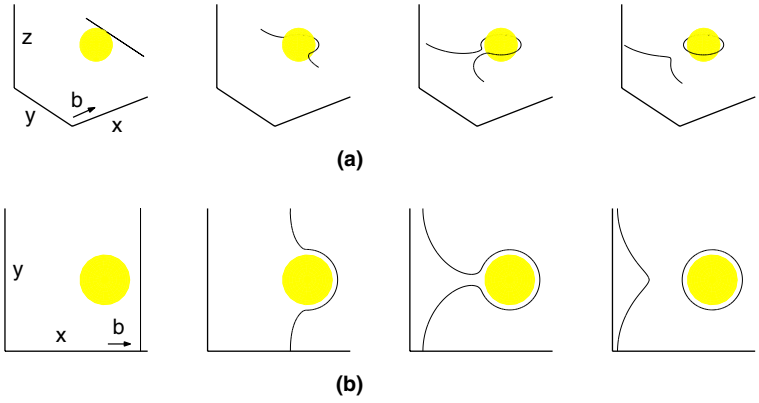

Fig. 2. An edge dislocation bypassing a hard spherical particle. The particle center lies on the slip plane of the dislocation, i.e., $h = 0$. (a) The top set of panels show a three-dimensional view at four times. (b) The bottom set corresponds to the same figures in the top panels, but viewed from above (i.e., looking in the $-z$ direction).

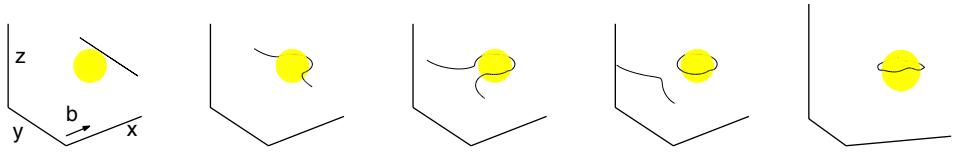

Fig. 3. The temporal evolution of an edge dislocation bypassing a hard spherical particle in a series of three-dimensional images. The initial slip plane of the dislocation is $h = 0.1R$ above the particle center.

forces on the screw segments with component in the $+z$ direction, causing cross-slip. At this height ($h = 0.1R$), the forces are not large enough to cause these segments to cross-slip all of the way around the particle. The last picture in Fig. 3 shows the equilibrium configuration of the loop. [2]

Next, we consider the case of an edge dislocation bypassing a particle in which the slip plane is $h = 0.5R$ above the particle center (see Fig. 4). The edge dislocation bypasses the particle by a combination of Orowan looping and cross-slip. Initially, as in the cases already discussed above, the dislocation approaches the particle under the action of the applied stress and begins to bend around the particle. When parts of the dislocation bend to be 90° relative to the original dislocation line (in the initial slip plane), two screw segments are formed on the sides of the particle. These screw segments begin to cross-slip up ($+z$ direction), while the dislocation continues to bend around the particle – eventually pinching-off to create a non-planar Orowan loop while the main dislocation moves on. The two cross-slipping screw segments, which are now part of the loop, continue to move over the top of the particle, annihilating one another. This creates non-glide loops in front of and behind the particle.

Note that although an Orowan loop forms in this process, it decays into two loops that do not lie in the initial slip plane of the edge dislocation. To our knowledge, this process has not previously been described, although a related process was discussed by Hirsch [2] and others [7,17–19] that produced a single loop behind the particle. This suggests that alternative bypass mechanisms are available depending on the relative magnitude of the self-stress (line tension) and the applied stress.

Fig. 5 shows a simulation of the case where the slip plane of the edge dislocation is $h = 0.75R$ above the particle center. The edge dislocation bypasses the particle by first bending partially around the particle, creating screw segments that cross-slip over the top of the particle and pinch-off, leaving a non-glide loop behind the particle as the dislocation moves on. No Orowan loop is created in this process. This case was observed and discussed by Hirsch and others [2,7,17–19].

3.2. Screw dislocations

We now examine the case of an initially straight screw dislocation bypassing a hard spherical particle. This presentation parallels that for the edge dislocation present above. In all cases, the Burgers vector **b** is in the $+y$ direction and the applied shear stress is $\sigma_{yz} = 4.0$.

In the $h = 0$ case, the dislocation bends around the particle and pinches-off to form an Orowan loop, as the

[2] We define an equilibrium state as a state where the average velocity of the dislocation over a long time is very small (i.e., less than 0.01 of that of the initial straight dislocation).

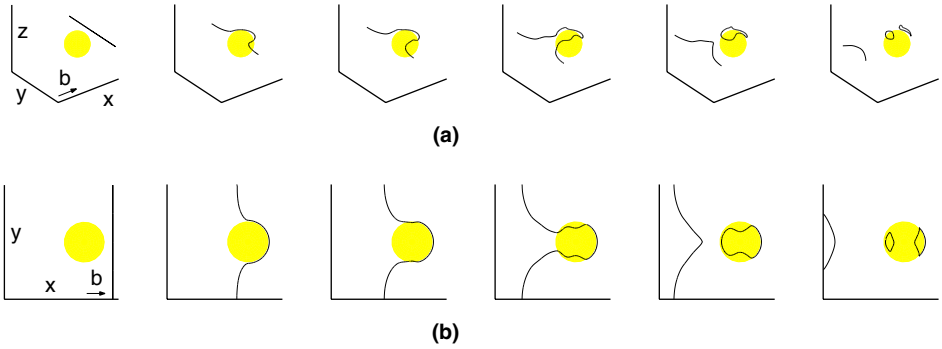

Fig. 4. An edge dislocation bypassing a hard particle where the slip plane of the dislocation is $h = 0.5R$ above the particle center. (a) The top set of panels show a three-dimensional view. (b) The bottom set is viewed from above (i.e., looking in the $-z$ direction) at the same times.

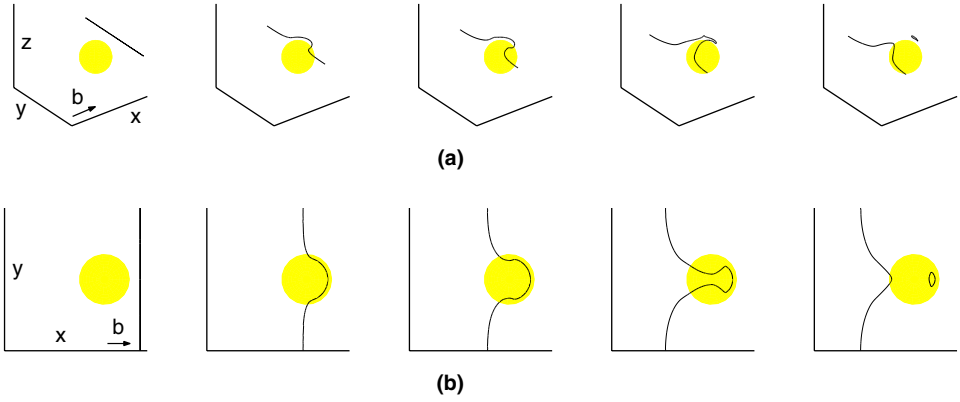

Fig. 5. An edge dislocation bypassing a hard particle where the slip plane of the dislocation is $h = 0.75R$ above the particle center. (a) The top set of panels show a three-dimensional view. (b) The bottom set is viewed from above (i.e., looking in the $-z$ direction) at the same times.

screw dislocation moves on (pictures for this case are indistinguishable from those in Fig. 2). Since there are no forces on any dislocation segment in the z direction, no cross-slip occurs and the loop formed is planar. This is the classical Orowan mechanism, discussed above, for an edge dislocation.

Fig. 6 shows a simulation of the case where the slip plane of the screw dislocation is slightly ($h = 0.1R$) above the particle center. The bypass process is similar to that in the $h = 0$ case. The dislocation bypasses the particle by Orowan mechanism, leaving behind a dislocation loop. However, the loop left behind does not lie entirely in the initial slip plane. The two screw segments on the loop (in front of and behind the particle) cross-slip out of the initial slip plane. In simple terms, this cross-slip is caused by the line tension of the dislocation loop and the broken symmetry of the problem associated with the fact that the nominal slip plane lies above the particle center. The last figure in the panel of Fig. 6 corresponds to an equilibrium state, where the cross-slip force is balanced by the line tension that resists forming long segments to connect the cross-slipping screw segments back to the remainder of the loop.

When the initial slip plane is displaced from the particle center by $h = 0.5R$, the cross slip forces are larger than in the previous ($h = 0.1R$) case. Fig. 7 shows the simulated bypass mechanism for this case. The screw dislocation bypasses the particle by a combination of Orowan looping and cross-slip. The screw dislocation approaches the particle under the action of the applied

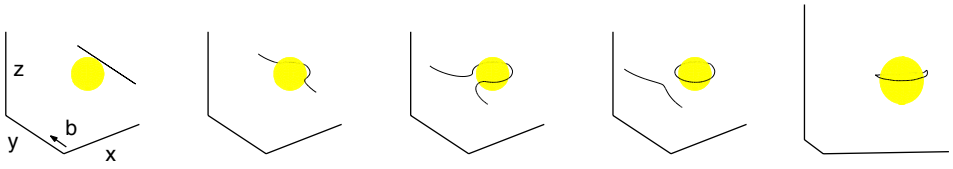

Fig. 6. A screw dislocation bypassing a hard particle where the slip plane of the dislocation is $h = 0.1R$ above the particle center.

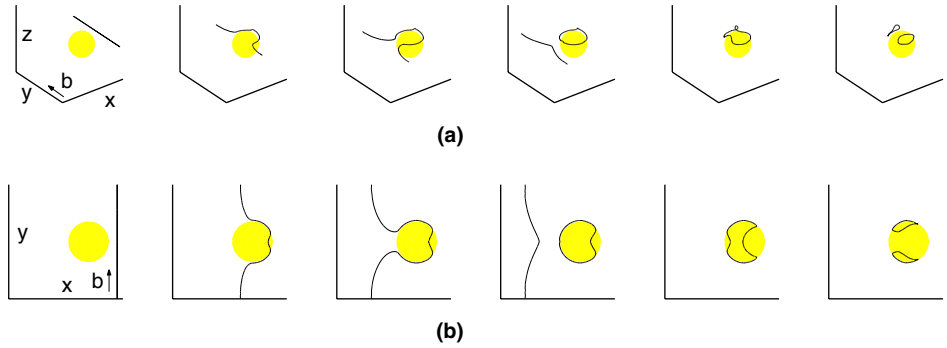

Fig. 7. A screw dislocation bypassing a hard particle where the initial slip plane is $h = 0.5R$ above the particle center. (a) The top set of panels show a three-dimensional view. (b) The bottom set is viewed from above (i.e., looking in the $-z$ direction) at the same times.

stress and begins to bend around the particle. The segments that begin to bend have some edge character and cannot cross-slip. On the other hand, the segment behind the particle remains in screw orientation and begins to cross-slip over the particle under the applied stress and its interaction with the non-coplanar particle. At the same time, the dislocation continues to bend around the particle and pinches-off an Orowan loop. Since this loop does not lie in the plane containing the particle center, the screw segment formed when the Orowan loop pinched-off begins to cross-slip over the top of the particle. The screw segments from in front of and behind the particle are attracted toward each other and annihilate. This leaves behind two non-glide loops on the two sides of the particle. Hirsch and Humphreys [7] and Humphreys and Martin [18] considered a similar case but suggested that double loop generation (as shown here) occurs by either the passage of a pair of screw dislocations or by the original screw segment undergoing triple cross-slip (i.e., without the initial formation of an Orowan loop).

4. Misfitting spherical particles

We now turn to the case where the particle has a dilatational misfit with respect to the matrix and can be penetrated (cut) by the dislocation. In this case, the dislocation-particle interactions are associated with the misfit stress field, as described by Eqs. (17) and (18). The misfit stress field outside the particle (17) provides not only a glide force, but can also lead to cross-slip of the screw segments. Clearly, these forces could also lead to dislocation climb; a situation we do not consider here. The stress inside the particle (18), is purely hydrostatic. While this can give rise to climb forces, it produces no glide forces. Situations do, however, occur where such forces exist – including when the particle/misfit are not isotropic and when the cutting dislocation leaves behind planar faults. In the present analysis, there are no interactions between particles and dislocation segments in their interior.

In the present simulations, the particle center is at $(x_0, y_0, z_0) = (0.1, 0, 0)$ and its radius is $R = 0.4$. Initially, the dislocation (edge or screw) is straight and located at $x = 0.9$ and $z = h$, pointing in the $+y$ direction. The dislocation moves towards the particle under an applied stress. We vary the relative positions of the particle and the slip plane of the dislocation by varying h, which is the signed distance from the particle center to the dislocation slip plane. Unlike in the case of hard spherical particles, the bypass mechanism for the edge dislocation is different depending on whether the slip plane is above or below the particle center (i.e., $+h$ is not equivalent to $-h$). We choose the misfit parameter $\epsilon = 0.02$.

4.1. Edge dislocations

In this section, we present the simulation results for an edge dislocation with Burgers vector $\mathbf{b}$ in the $+x$ direction and an applied shear stress of $\sigma_{xz} = 4.0$. There is no interaction between the particle and the dislocation segment inside it. Outside the particle the force on the dislocation due to the misfit stress is given by the Peach–Koehler force $\mathbf{f} = \sigma^{\mathrm{pt}} \cdot \mathbf{b} \times \xi$, where ξ is the tangent vector of the dislocation and σ^{pt} is the misfit stress. Using Eq. (17) to describe the misfit stress and with $\mathbf{b}$ in the $+x$ direction, we have

$$\begin{aligned}\sigma^{\mathrm{pt}} \cdot \mathbf{b} &= b(\sigma^{\mathrm{pt}}_{xx}, \sigma^{\mathrm{pt}}_{xy}, \sigma^{\mathrm{pt}}_{xz}) \\ &= \frac{2Gb\epsilon R^3}{r^5}\Big(r^2 - 3(x-x_0)^2, -3(x-x_0)(y-y_0), \\ &\quad -3(x-x_0)(z-z_0)\Big), \end{aligned} \tag{19}$$

where $r = \sqrt{(x-x_0)^2 + (y-y_0)^2 + (z-z_0)^2}$ is the distance from a point in space (x, y, z) to the center of the particle $(x_0, y_0, z_0) = (0.1, 0, 0)$. The straight edge dislocation initially lies on a slip plane with normal in the z direction, so $\sigma^{\mathrm{pt}}_{xz}$ creates a glide force, $\sigma^{\mathrm{pt}}_{xy}$ creates a cross-slip force for the screw segments, and $\sigma^{\mathrm{pt}}_{xx}$ creates a climb force (not considered here). In the present simulations, we chose $\epsilon = 0.02 > 0$. If we let $\epsilon \to -\epsilon$, the results are unchanged provided that we also set $h \to -h$.

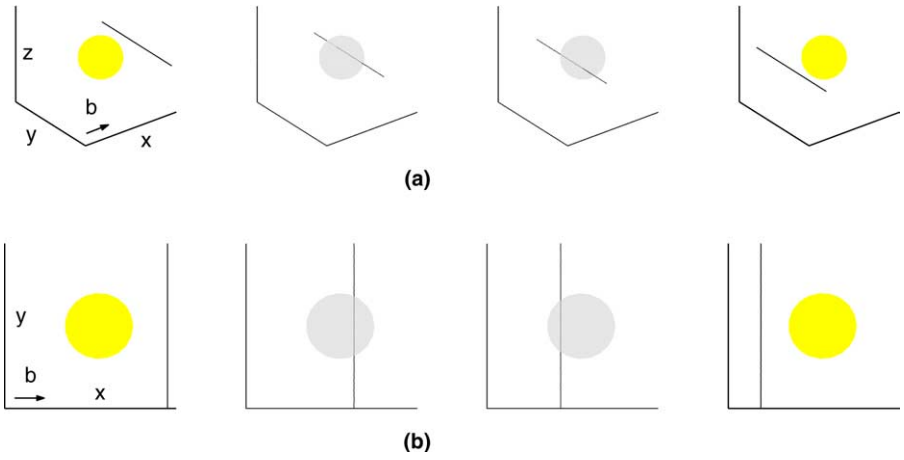

Fig. 8. An edge dislocation bypassing a misfitting spherical particle where the particle center is on the slip plane of the dislocation, i.e., $h = 0$. (a) The top set of figures show a three-dimensional view at different times during the evolution. (b) The bottom set shows the same figures viewed from above (i.e., looking in the $-z$ direction). Note that some of the particles in this and subsequent figures are made semi-transparent in order to make it easier to determine the location of the dislocation segments inside or behind the particles.

Fig. 8 shows a simulation of the motion of the edge dislocation for the case where the particle center lies on the initial slip plane, i.e., $h = 0$. Because of the symmetry of this situation, $\sigma_{xz}^{\mathrm{pt}} = 0$ along the entire slip plane. This implies that the misfit stress does not modify the glide force on the edge dislocation. Therefore, the dislocation remains straight before, after and while it cuts through the misfitting particle.

We now examine two cases in which the initial slip plane is only very slightly above (Fig. 9) or below (Fig. 10) the center of the particle. In these cases, the shear stress associated with misfitting particle $\sigma_{xz}^{\mathrm{pt}}$ in the initial slip is non-zero, but very small. This suggests that there will be a weak glide force on the dislocations associated with the the particle misfit. In these cases, the dislocation can still cut through the particle. In the $h = 0.0375R > 0$ case, the dislocation is weakly repelled from the particle, while in the $h = -0.0375R < 0$ case it is weakly attracted towards the particle. As a result, the dislocation shown in Fig. 9 bows away from the particle center, while in the case shown in Fig. 10 it bows towards the particle center.

Fig. 11 shows the simulated motion of an edge dislocation bypassing the misfitting particle for the case in which the initial slip plane is $h = 0.5R$ above the center of the particle. In this case, the shear stress associated with the particle misfit that couples to edge dislocation glide in the slip plane $\sigma_{xz}^{\mathrm{pt}}$ gives rise to a strong repulsive force (see Eq. (19)). The edge dislocation stands-off from the particle as it begins to bend around (see the second image in each row in Fig. 11). The misfit stresses drive the screw segments of the bowed dislocation to cross-slip on the sides of the particle. The direction of the cross-slip depends on the position of the screw segment relative to the x-coordinate of the particle center (i.e., (x_0, y_0, z_0)): the $x > x_0$ segment cross-slips in the $-z$

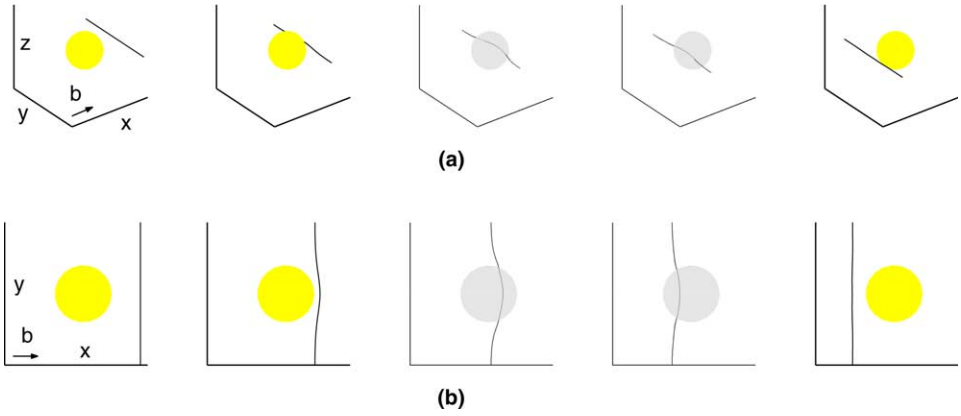

Fig. 9. An edge dislocation bypassing a misfitting spherical particle where the slip plane of the dislocation is slightly above the particle center, $h = 0.0375R$. (a) The top set of figures show a three-dimensional view at different times during the evolution. (b) The bottom set shows the same figures viewed from above (i.e., looking in the $-z$ direction).

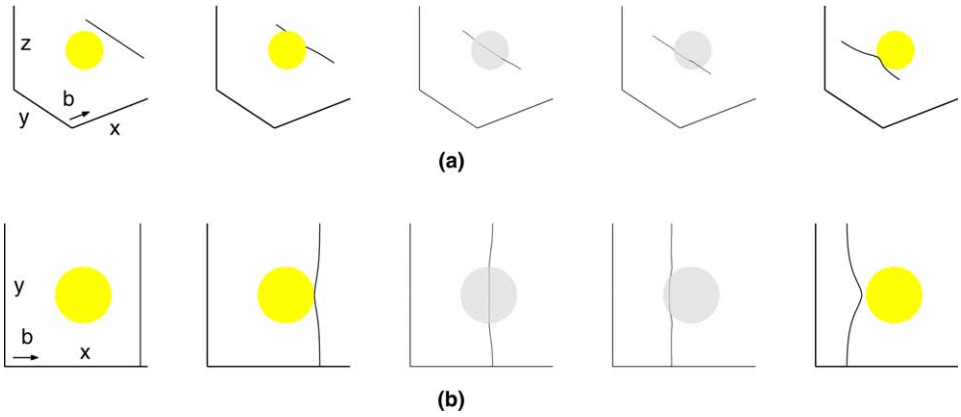

Fig. 10. An edge dislocation bypassing a misfitting spherical particle where the slip plane of the dislocation is slightly below the particle center, $h = -0.0375R$. (a) The top set of figures show a three-dimensional view at different times during the evolution. (b) The bottom set shows the same figures viewed from above (i.e., looking in the $-z$ direction).

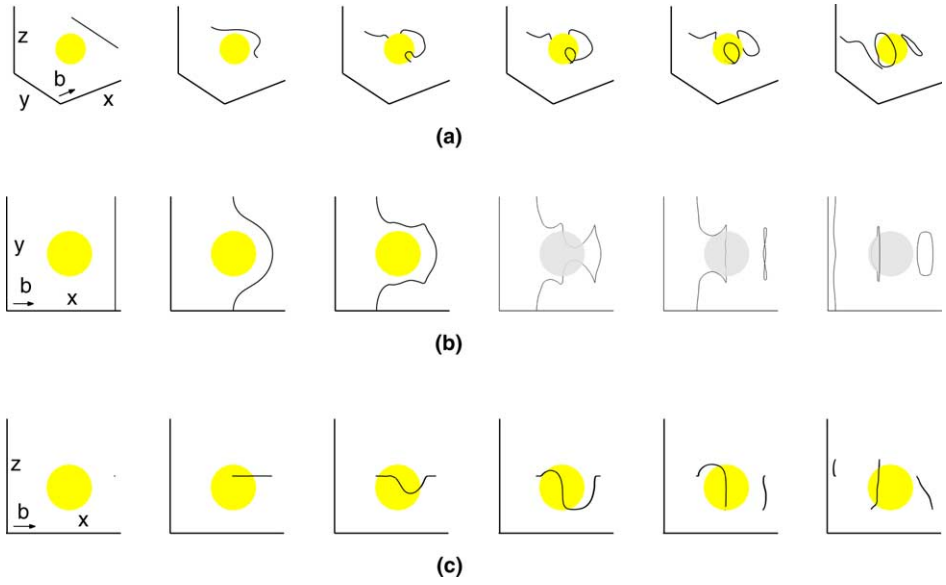

Fig. 11. An edge dislocation bypassing a misfitting spherical particle where the slip plane of the dislocation is $h = 0.5R$ above the particle center. (a) The top set of figures show a three-dimensional view at different times during the evolution (b) The middle set shows the same figures viewed from above (i.e., looking in the $-z$ direction). (c) The bottom set shows the same figures viewed from side (i.e., looking in the $+y$ direction).

direction and the $x < x_0$ cross-slips in the $+z$ direction (see the third and fourth images in each row in Fig. 11). This is consistent with the change in sign of $\sigma^{pt} \cdot \mathbf{b}$ in Eq. (19) when the dislocation passes the point $x = x_0$. The two cross-slipped screw segments at $x > x_0$ are attracted towards each other under the particle and annihilate there (see the fifth image in each row in Fig. 11). The two cross-slipped screw segments at $x < x_0$ are attracted towards each other and annihilate above the particle (see the sixth image in each row in Fig. 11). This process creates two non-glide loops, initially parallel to the yz-plane (at later times they move out of this plane). The two loops (obviously) have the same Burgers vector but the line directions are in the opposite sense from one another. This implies that the dislocation loops are interstitial and vacancy loops.

This mechanism was proposed by Humphreys and Hirsch in the context of alumina particles in a copper matrix [19]; however, they found no evidence for the operation of this mechanism in these alloys. Duesbery and Sadananda [12] calculated the shape of an edge dislocation bypassing a particle under conditions similar to those simulated here and observed Orowan loop formation. The present simulations demonstrate that cross-slip does occur early, thereby preventing the formation of Orowan loops. This discrepancy can be traced to two factors: first, the present simulations were performed with a relatively large misfit strain and,

second, Duesbery and Sadananda constrained the dislocation to move in a fixed slip plane and did not consider cross-slip at all.

The next figure (Fig. 12) shows a simulation of the case where the slip plane of the edge dislocation is below the particle center, at $h = -0.5R$. While this case only differs from the previous one (Fig. 11) by the sign of the displacement of the initial slip plane from the particle center, the bypass mechanism is entirely different. In this case, the shear stress in the slip plane due to the misfitting particle σ^{pt}_{xz} generates a strong force that initially attracts the dislocation towards the particle (see Eq. (19)). The dislocation begins to cut the particle. The segments outside, but near the particle, continue to be pulled forward, while the segment inside the particle lags behind because the particle produces no drive on internal dislocation segments (see the third image in each row in Fig. 12). Next, the dislocation cuts the remaining distance through the particle, but because of the attraction to the particle, remains against the far particle surface (i.e., $x < x_0$), as shown in the fourth image in each row in Fig. 12. As the dislocation continues to be pulled forward by the external stress, the segments on the side of the particle cross slip upward (fifth image) and pinch-off on the upper surface of the particle (sixth image). This creates a non-glide loop, as the remainder of the dislocation continues to move on. This case was also considered by Duesbery and Sadananda [12]. They predicted the formation of an Orowan loop that cuts through half of the particle. The differences between their predictions and those from the present simulations were discussed in the previous paragraph.

Figs. 13 and 14 show the motion of edge dislocations with slip planes far above ($h = 1.825R$) and far below ($h = -1.825R$) the particle center. Since the interaction between the dislocation and the misfit particle is through a long-range elastic field, the presence of the particle is able to distort the passing dislocation line, thereby producing an increment in the yield strength of the material. In the $h = 1.825R > 0$ case, the dislocation is repelled from the particle and hence bows away from it. When the dislocation passes below the particle ($h = -1.825R < 0$), the dislocation is attracted toward the particle and hence bows towards it. In these cases, the particles can be viewed as either simple potential barriers or potential wells, past which the dislocations must be driven.

4.2. Screw dislocations

In this section, we present the simulation results for a screw dislocation bypassing a particle that is misfitting (dilatation) with respect to the matrix. The Burgers vector $\mathbf{b}$ is in the $+y$ direction and the applied shear stress is $\sigma_{yz} = 4.0$ in all of the examples shown. Outside the particle, the force due to the long-range misfit interaction is the Peach–Koehler force $\mathbf{f} = \sigma^{pt} \cdot \mathbf{b} \times \xi$, where ξ is the tangent vector of the dislocation, and

$$\begin{aligned}\sigma^{pt} \cdot \mathbf{b} &= b(\sigma^{pt}_{yx}, \sigma^{pt}_{yy}, \sigma^{pt}_{yz}) \\ &= \frac{2Gb\epsilon R^3}{r^5}\Big(-3(x-x_0)(y-y_0), r^2 - 3(y-y_0)^2, \\ &\quad -3(y-y_0)(z-z_0)\Big),\end{aligned} \tag{20}$$

where $r = \sqrt{(x-x_0)^2 + (y-y_0)^2 + (z-z_0)^2}$ is the distance from a point (x, y, z) to the center of the particle $(x_0, y_0, z_0) = (0.1, 0, 0)$. Recall that we chose the misfit parameter to be $\epsilon = 0.02$. The simulation cells are $2l \times l \times l$ discretized into $128 \times 64 \times 64$ grid points.

In the absence of a particle, the initially straight screw dislocation will slip on a plane parallel to the xy plane. The contribution of the particle to the glide force on this plane is proportional to σ^{pt}_{yz} and σ^{pt}_{yx} generates a force that drives cross-slip. Since the stress σ^{pt}_{yx} on the initial straight screw dislocation is non-zero, the screw is subject to cross-slip forces from the very beginning. Interestingly, in this case the segment of the dislocation at $y > y_0$ is forced downward (in the $-z$ direction) and the segment at $y < y_0$ is forced upward (in the $+z$ di-

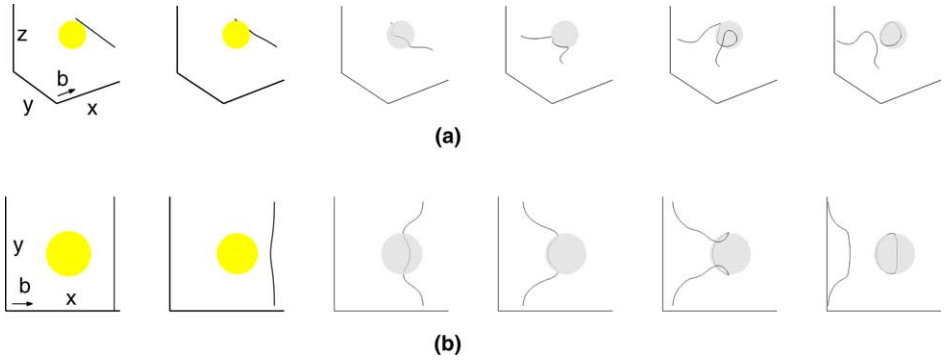

Fig. 12. An edge dislocation bypassing a misfitting particle where the slip plane of the dislocation is at $h = -0.5R$, below the particle center. (a) The top set of figures show a three-dimensional view at different times during the evolution. (b) The bottom set shows the same figures viewed from above (i.e., looking in the $-z$ direction).

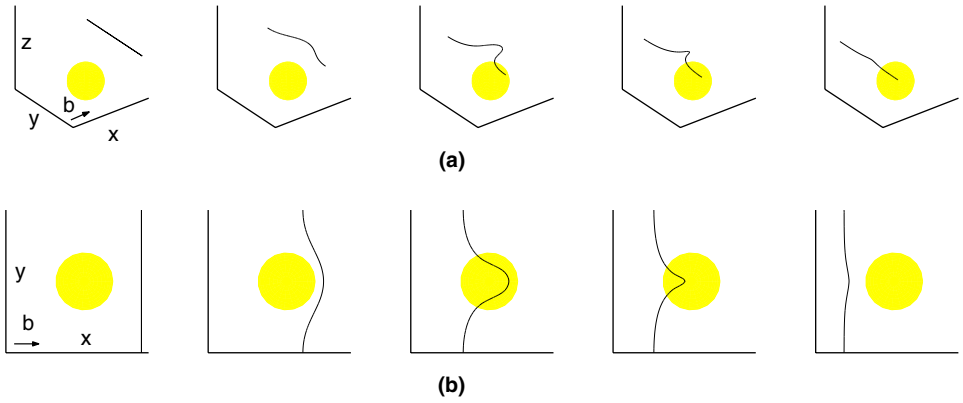

Fig. 13. An edge dislocation bypassing a misfitting particle where the slip plane of the dislocation is $h = 1.825R$ above the particle center. (a) The top set of panels show a three-dimensional view. (b) The bottom set is viewed from above (i.e., looking in the $-z$ direction).

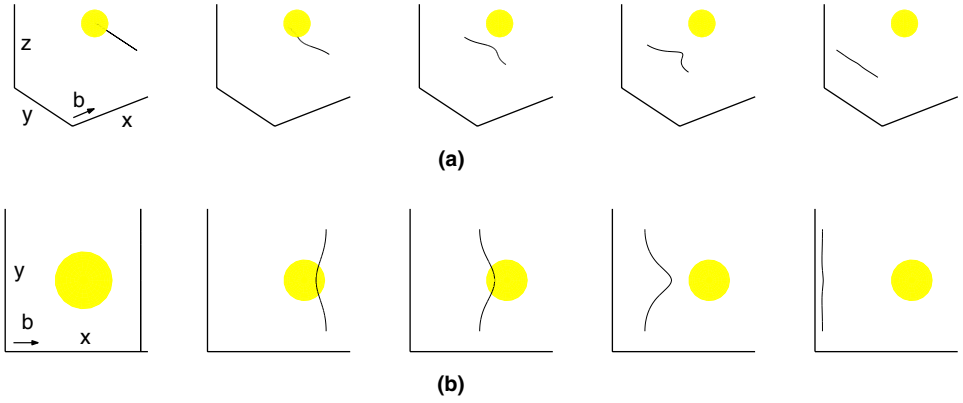

Fig. 14. An edge dislocation bypassing a misfitting particle where the slip plane of the dislocation is at $h = -1.825R$, below the particle center. (a) The top set of panels show a three-dimensional view. (b) The bottom set is viewed from below (i.e., looking in the $+z$ direction).

rection). The misfitting particle exerts no cross-slip (or glide) force on the screw dislocation at $y = y_0$. Once the dislocation passes the mid-plane of the particle ($x = x_0$), the sign of the cross-slip force on the screw segments switches. Recall that periodic boundary conditions are employed in the present simulations, such that the dislocation is actually moving past a regular array of particles. This implies that the sign of the cross-slip force also changes at the midpoint between two particles. In order to more clearly understand screw dislocations bypassing misfitting particles, we plot the configurations so as to show several particles from the particle array.

Fig. 15 shows a simulation of the case where the slip plane of the initially straight screw dislocation is $h = 1.5R$ above the particle center. As described above, on the left of the particle ($y < y_0$), the screw segment cross-slips upward ($+z$) as it moves forward ($-x$); while on the right of the particle ($y > y_0$), the screw segment cross-slips downward ($-z$) as it moves forward. However, because the dislocation is above the particle, the segment that cross-slips upward is longer than the segment that cross-slips downward. As the upper segments move forward past the particle, they pull the segments that initially cross-slipped downward up and over the particle. As the dislocation continues to move forward, it becomes increasingly straight.

Next, we consider the symmetric case of a screw dislocation with an initial slip plane that intersects the misfitting particle center, Fig. 16. As always in these screw dislocation figures, the screw segment to the left of the particle ($y < y_0$) cross-slips upward as it moves forward; while on the right of the particle ($y > y_0$), the screw segment cross-slips downward. This leads to the formation of edge dislocation segment behind the particle that is nearly vertical and centered at the mid-plane of the particle, $y = y_0$ plane (see the second image in each row of Fig. 16). The screw segment above the particle ($z > z_0 + R$) cross-slips over the top of the particle and the screw segment below the particle ($z < z_0 - R$) cross-slips below the bottom of the particle (see the second image). These screw segments continue to cross-slip around the particle (see the third image) until they meet in front of the particle ($x \approx x_0 - R$).

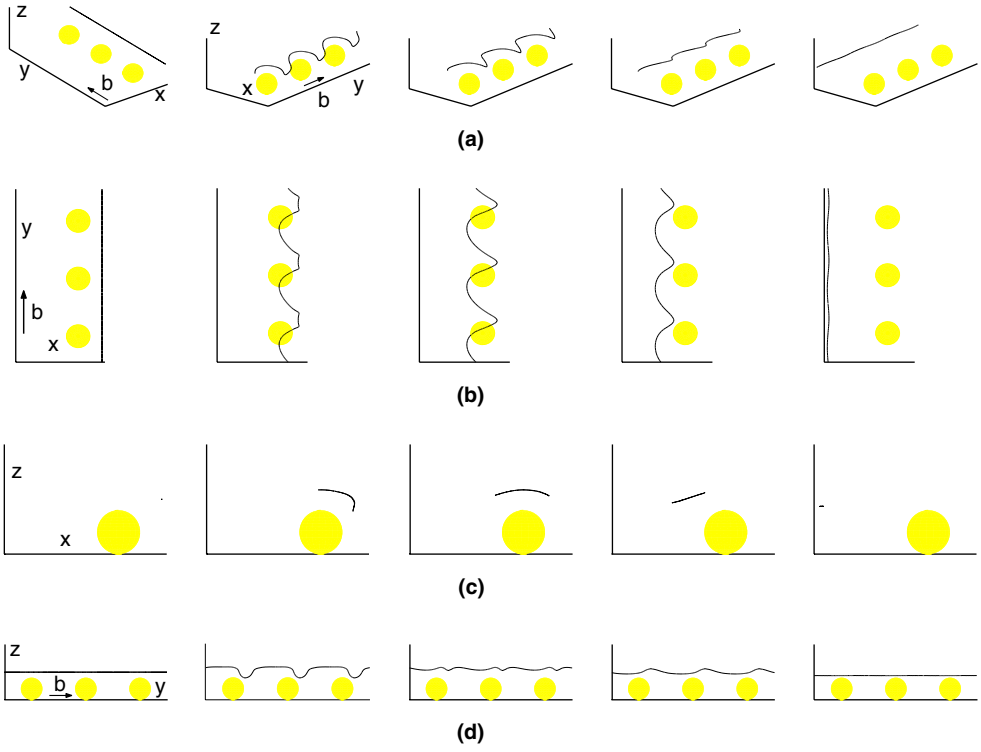

Fig. 15. A screw dislocation bypassing a regular misfitting particle array where the slip plane of the dislocation is $h = 1.5R$ above the particle center. (a) The top set of panels show a three-dimensional view, (b) the second set of panels are viewed from above (i.e., looking in the $-z$ direction), (c) the third set of panels are viewed from the side (i.e., looking in the $+y$ direction), (d) the bottom set is viewed from back (i.e., looking in the $-x$ direction), as indicated by the axes labels.

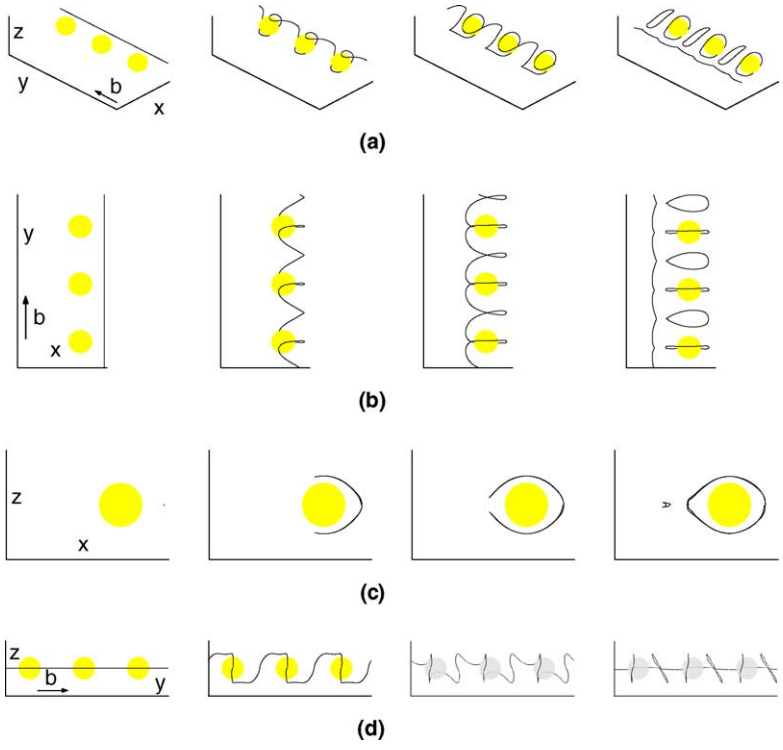

Fig. 16. A screw dislocation bypassing a regular misfitting particle array where the slip plane of the dislocation cuts through the center of the particle, $h = 0$. (a) The top set of panels show a three-dimensional view, (b) the second set of panels are viewed from above (i.e., looking in the $-z$ direction), (c) the third set of panels are viewed from the side (i.e., looking in the $+y$ direction), (d) the bottom set is viewed from the back (i.e., looking in the $-x$ direction), as indicated by the axes labels.

This pinches-off a prismatic dislocation loop at $y = y_0$ centered at the mid-point of the particle (see the fourth image). Interestingly, the geometry of this dislocation line necessitates the simultaneous formation of a similar, but oppositely signed, parallel, (nearly) prismatic loop between the particles.

Fig. 17 shows an initially straight screw dislocation with an initial slip plane $h = 1.25R$ above the center of a misfitting particle. The initial evolution of the shape of the dislocation line is very similar to that shown for $h = 0$ (see the first three images in Fig. 16). However, unlike in the $h = 0$ case, this one is less symmetric. Instead of the dislocations pinching-off a loop around the particle in the $y = y_0$ plane, the pinch-off occurs above the particles (i.e., $z > z_0 + R$). This produces a non-planar loop around the particle, nominally with a normal in the z direction. Because of where the pinch-off occurs, there are only half as many loops created as in the $h = 0$ case.

Even after the dislocation moves well past the array of particles and set of loops form, the structure may continue to evolve as a result of the dislocation-particle, dislocation–dislocation and dislocation-applied stress interactions. An interesting example of this is shown in Fig. 18, in which the initial slip plane of the screw dislocation intersects the top of the misfitting particles ($h = R$). At first, the dislocation structure evolves in a manner that is very similar to that shown for the $h = 0$ case (Fig. 16), above. The dislocation segment wrapping around the upper part of the particle and the segment wrapping around lower part of the particle meet and the dislocation bypasses the particles leaving a loop around each particle (in the $y = y_0$ plane) and an oppositely signed loop between the adjacent particles (see the first four images in both rows of Fig. 18). The continuous screw dislocation then moves out of the field of view of the figures and every pair of loops react to form a single loop (see images 5 and 6 in Fig. 18). These new loops then react with one another, destroying all of the loops and creating a new screw dislocation with the same sense as the original screw dislocation to the left of the particles ($x < x_0$) plus another dislocation with the opposite sense around the particles (image 7). Because of the misfit stress field, the latter dislocation wraps around the particles again, generates two new loops per particle (images 8 and 9) plus a dislocation of the opposite sense which moves away in the $+x$ direction. This interesting process starts with a single screw dislocation, generates a large series of loops plus two new dislocations of opposite sign. This is a new dislocation generation mechanism that is unique to misfit particles.

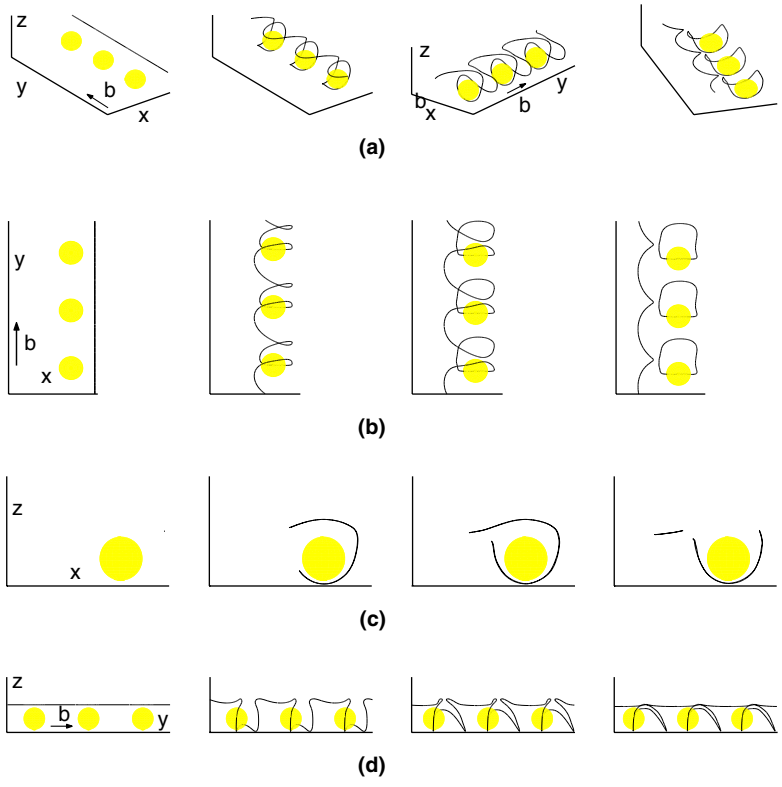

Fig. 17. A screw dislocation bypassing a regular array of misfitting particles where the slip plane of the dislocation is $h = 1.25R$ above the particle centers. (a) The top set of panels show a three-dimensional view, (b) the second set of panels are viewed from above (i.e., looking in the $-z$ direction), (c) the third set of panels are viewed from the side (i.e., looking in the $+y$ direction), (d) the bottom set is viewed from the back (i.e., looking in the $-x$ direction), as indicated by the axes labels.

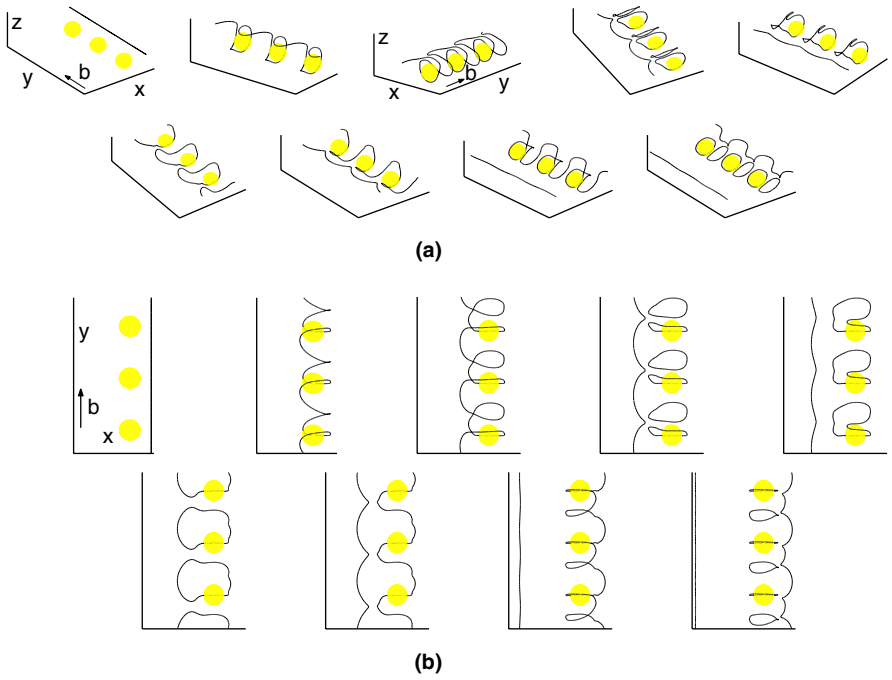

Fig. 18. A screw dislocation bypassing a regular array of misfitting particles where the slip plane of the dislocation intersects the top of the particles $h = R$. (a) The top set of panels show a three-dimensional view. (b) The bottom set of panels are viewed from above (i.e., looking in the $-z$ direction).

Duesbery and Sadananda [12] also simulated the case of a screw dislocation bypassing penetrable, misfitting particles. In their simulations, the dislocation was constrained to a single plane ($h = 0.7R$), such that cross-slip was prevented. Because of the misfit, they found that an edge segment cut through and stopped in the center of the particle (lying parallel to y). The dislocation bypassed the particle by forming a loop; partly inside and partly outside the particle (see their Fig. 10b). For the same conditions, we generate a dislocation configuration similar to Fig. 16, in which the screw dislocation undergoes extensive cross-slip and generates a pair of dislocation loops roughly perpendicular to the initial slip plane. These starkly different scenarios indicate the importance of considering the dislocation dynamics in three dimensions and the importance of including cross-slip.

5. Hard misfitting particles

To this point, we have considered edge and screw dislocations interacting with hard (impenetrable) particles and interacting with penetrable, misfitting particles. In this section, we consider a combination of these two cases – i.e., edge and screw dislocations bypassing an array of impenetrable, misfitting spherical particles. This involves both long-range misfit stress interactions and short-range repulsive interactions between the dislocation and the particle. The long-range, misfit interaction between the dislocation and the particle is described by Eqs. (17) and (18) and the short-range, repulsive interaction between the dislocation and the particle by Eq. (16). Not surprisingly, the simulation results are similar to those of the penetrable, misfitting particles shown above, except that the dislocation cannot enter the particle itself, as commonly occurred (see Figs. 8–18). The particle cutting is replaced by looping and/or cross-slip.

As in the simulations for the penetrable, misfitting particle, the $R = 0.4$ particle has a misfit of $\epsilon = 0.02$ with respect to the matrix and is centered at $(x_0, y_0, z_0) = (0.1, 0, 0)$. Initially, the dislocation (edge or screw) is straight and located at $x = 0.9$ and $z = h$, with the line direction in the $+y$ direction. The dislocation moves towards the particle under an applied stress.

5.1. Edge dislocations

We begin with an edge dislocation with a Burgers vector **b** in the $+x$ direction and an applied shear stress of $\sigma_{xz} = 4.0$. The $h = \pm 1.825R$ cases are exactly the same as those of the penetrable misfitting particles (see Figs. 13 and 14), since in these cases, the dislocations never penetrate the particles. The $h = 0.5R$ case is also unchanged with respect to the corresponding penetrable, misfitting particle case (see Fig. 11) because of the strong repulsive misfit interaction between the dislocation and the particle, which prevents the dislocation from entering into the particle. On the other hand, the present $h = 0$ case is completely different from that of the penetrable misfitting particle, in which the dislocation-

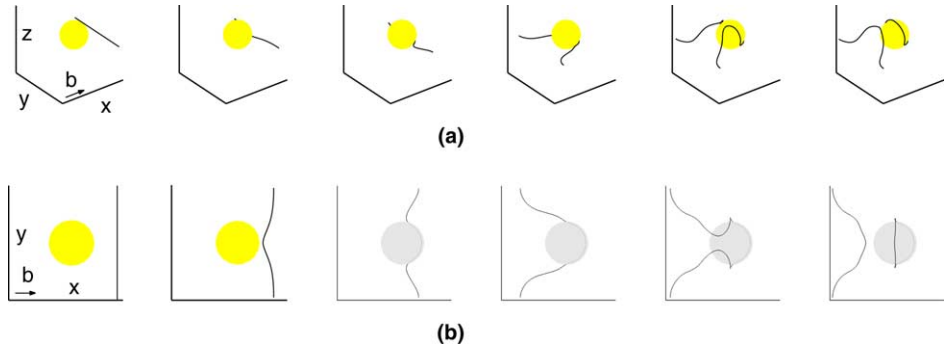

Fig. 19. An edge dislocation bypassing an impenetrable misfitting particle where the initial slip plane is $h = -0.5R$ below the particle center. (a) The top set of images show a three-dimensional view. (b) The bottom set is viewed from above (i.e., looking in the $-z$ direction).

particle interaction is zero and the dislocation cuts straight through the particle (see Fig. 8). Rather, this case is nearly identical with the $h = 0.5R$ case for the penetrable particle: the dislocation bypasses the particle via a complex mechanism and leaves behind two non-glide loops with opposite signs near the particle (see Fig. 11). The main difference is that while the dislocation does not cut the particle because of the long-range repulsive misfit interaction in the penetrable particle ($h = 0.5R$ case, Fig. 11), in the present case ($h = 0$) the dislocation cannot cut the particle due to the short-range repulsive interaction. Accordingly, the dislocation bends before it reaches the particle in the $h = 0.5R$ case (Fig. 11) and does not bend until the dislocation hits the particle in the $h = 0$ impenetrable particle case. Once bending begins, the two cases are very similar.

The $h = -0.5R$ case is shown in Fig. 19. This should be compared with the penetrable particle case (see Fig. 12). Although the bypass mechanisms in the two cases are quite different, the final dislocation configurations are remarkably similar. In the penetrable particle case, the dislocation cuts all of the way through the particle, then cross-slips around the particle. This leaves a loop which is half-prismatic ($z > z_0 + h$) and half-glide ($x < x_0$). In the impenetrable particle case, the edge dislocation starts to bend around the particle, then cross-slips upward and pinches-off. This leaves a loop which is half-prismatic ($z > z_0 + h$) and half-glide. The main difference is that in this case, the half-glide loop lies on the opposite side of the particle, ($x > x_0$).

5.2. Screw dislocations

For a screw dislocation, the dislocation bypass mechanisms and configurations for the impenetrable, misfitting particles are, in all cases, essentially identical with those for the corresponding penetrable misfitting particles, as described in the previous section. This can be understood by noting that in the penetrable, misfitting particle cases, the dislocation always remains outside of the particle as a result of the long-range misfit interactions.

6. Discussion

The present simulations demonstrate the richness and complexity of the mechanisms by which dislocations bypass arrays of particles. We have observed both particle cutting, dislocation loop formation and combinations of these. Loop formation is particularly interesting. We have shown examples of loops formed in front of and behind particles, on the sides of particles, in between particles, around particles and as combinations of these. The loops around particles can be either in the dislocation glide plane, as in the classical Orowan mechanism, or in either of the two planes orthogonal to this one. Since there are several different mechanisms that can produce nearly identical loops, caution must be used in trying to deduce bypass mechanisms from postmortem analysis of deformation microstructures. Examination of the simulated dislocation microstructures that remain following particle bypassing with experimental observations indicates striking similarities (see e.g. [7,18,19]), as discussed above.

One novel result of the present simulations was the discovery of a new dislocation generation mechanism. In particular, we observed that a screw dislocation bypassing an array of misfitting particles can generate an array of nearly prismatic loops of both signs (see Fig. 18). These loops can interact with each other to generate a dislocation of the same sign as the original, thereby destroying the loops, and a dislocation of the opposite sign as the original, thereby recreating the loops. Since this observation was serendipitous, we must conclude that there are a wide range of bypass mechanisms and geometries that can generate new dislocations.

In the present work, we only examined the case of a regular array of particles, in nature particle arrays are always much more disordered. Further, we have only examined the case of a dislocation bypassing pristine particles, whereas in deformation experiments dislocations bypass particles and the debris left behind by previous dislocations. Finally, we have described particles only in terms of their penetrability and misfit, while in many alloys it is also important to include effects

associated with elastic inhomogeneity (i.e., modulus mismatch), the condition of the particle-matrix interfaces (slipping or non-slipping), their shape and their crystallography. Therefore, we view the richness of the observed bypass mechanisms observed here to represent only a small glimpse into the deformation of realistic, multiphase alloys. Each of these areas requires more careful study.

It is important to mention a few of the limitations of the present simulation approach. First, the numerical methods used in the present simulations are not effective in keeping sharp features along the dislocation line sharp (e.g., the corners resulting from the cross-slip of a dislocation segment). This results in all of the dislocation lines and loops in the figures being much smoother than they should be. Second, the current methods do not completely prevent the motion of dislocations out of their slip plane even though the climb mobility is set to zero. Although such motion is very slow, it should not occur at all. This type of motion is equivalent to having a very small climb mobility. In addition to these numerical issues, there are some aspects of the physics that we do not include. For example, we do not consider the crystallography of slip, but rather let a dislocation move in any plane that contains the Burgers vector and line direction. This makes cross-slip very easy, contributes to smoother dislocations than routinely observed in crystals and limits the effects of crystallography to only the choice of Burgers vectors.

Acknowledgements

The authors gratefully acknowledge the support of the National Science Foundation through Grant DMR0080766 and the Defense Advanced Research Project Agency through Grant F33615-01-2-2165. The third author was supported in part by NSF Grant #0208449.

References

[1] Orowan E. Symposium on Internal Stress in Metals and Alloys, The Institute of Metals, London, 1948, p. 451.
[2] Hirsch PB. J Inst Met 1957;86:13.
[3] Friedel J. Les dislocations. Paris: Cauthier-Villars; 1956.
[4] Ashby MF. Acta Metall 1966;14:679.
[5] Kocks UF. Can J Phys 1967;45:737.
[6] Gleiter H. Acta Metall 1967;15:1213.
[7] Hirsch PB, Humphreys FJ. In: Argon AS, editor. Physics of strength and plasticity. Cambridge (MA): MIT Press; 1969.
[8] Foreman AJE, Makin MJ. Philos Mag 1966;14:911.
[9] Bacon DJ, Kocks UF, Scattergood RO. Philos Mag 1973;28:1241.
[10] Scattergood RO, Bacon DJ. Philos Mag 1975;31:179.
[11] Schwarz RB, Labusch R. J Appl Phys 1978;49:5174.
[12] Duesbery MS, Sadananda K. Philos Mag 1991;63:535.
[13] Fuchs A, Ronnpagel D. Mater Sci Eng A 1993;164:340.
[14] Mohles V, Ronnpagel D, Nembach E. Comput Mater Sci 1999;16:144.
[15] Mohles V. Mater Sci Eng A 2001;309–310:265.
[16] Mohles V. Mater Sci Eng A 2001;319–321:201.
[17] Ashby MF, Smith GC. Philos Mag 1960;5:298.
[18] Humphreys FJ, Martin JW. Philos Mag 1967;16:927.
[19] Humphreys FJ, Hirsch PB. Proc Roy Soc Lond A 1970;318:73.
[20] MacEwen SR, Hirsch PB, Vitek V. Philos Mag 1973;28:703.
[21] Xiang Y, Cheng LT, Srolovitz DJ, E W. Acta Mater 2003;51:5499.
[22] Nabarro FRN. Theory of crystal dislocations. Oxford (UK): Clarendon Press; 1967.
[23] Hirth JP, Lothe J. Theory of dislocations. 2nd ed. New York: Wiley; 1982.
[24] Lardner RW. Mathematical theory of dislocations and fracture. Toronto and Buffalo: University of Toronto Press; 1974.
[25] Landau LD, Lifshitz EM. Theory of elasticity. 3rd ed. New York: Pergamon Press; 1986.
[26] Osher S, Sethian JA. J Comput Phys 1988;79:12.
[27] Burchard P, Cheng LT, Merriman B, Osher S. J Comput Phys 2001;170:720.
[28] Osher S, Fedkiw RP. J Comput Phys 2001;169:463.
[29] Bulatov VV. J Comput Aided Mater Des 2002;9:133.
[30] Bulatov VV, Rhee M, Cai W. In: Kubin L et al., editors. Multiscale modeling of materials-2000. Warrendale (PA): Materials Research Society; 2001.
[31] Jiang GS, Peng D. SIAM J Sci Comput 2000;21:2126.
[32] Spiteri RJ, Ruuth SJ. SIAM J Numer Anal 2002;40:469.
[33] Eshelby JD. In: Seitz F, Turnbull D, editors, Solid state physics, vol. 3. New York: Academic Press; 1956.